RSC Advances

This is an *Accepted Manuscript*, which has been through the Royal Society of Chemistry peer review process and has been accepted for publication.

Accepted Manuscripts are published online shortly after acceptance, before technical editing, formatting and proof reading. Using this free service, authors can make their results available to the community, in citable form, before we publish the edited article. This *Accepted Manuscript* will be replaced by the edited, formatted and paginated article as soon as this is available.

You can find more information about *Accepted Manuscripts* in the Information for Authors.

Please note that technical editing may introduce minor changes to the text and/or graphics, which may alter content. The journal's standard Terms & Conditions and the Ethical guidelines still apply. In no event shall the Royal Society of Chemistry be held responsible for any errors or omissions in this *Accepted Manuscript* or any consequences arising from the use of any information it contains.

ROYAL SOCIETY OF CHEMISTRY

www.rsc.org/advances

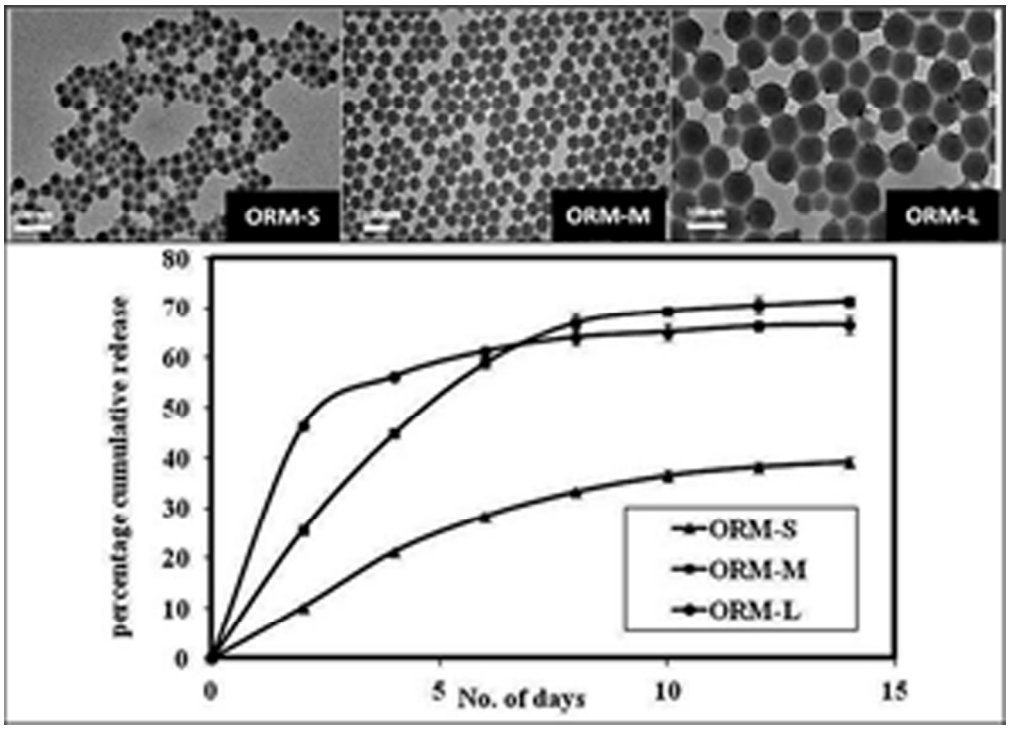

TEM images (above) and release profiles (below) of encapsulated drug from ormosil nanoparticles with small (ORM-S), medium (ORM-M) and large (ORM-L) sizes
76x54mm (300 x 300 DPI)

RSC Advances Accepted Manuscript

Cite this: DOI: 10.1039/c0xx00000x

www.rsc.org/xxxxxx

ARTICLE

Ormosil nanoparticles as a sustained-release drug delivery vehicle

Indrajit Roy[a]*, Pramod Kumar[a], Rajiv Kumar[b], Tymish Y. Ohulchanskyy[b], Ken-Tye Yong[c], and Paras N Prasad[b]*

Received (in XXX, XXX) Xth XXXXXXXXX 20XX, Accepted Xth XXXXXXXXX 20XX
DOI: 10.1039/b000000x

Abstract

Silica-based nanoparticles are well known for their ease of synthesis, structural robustness, resistance to biofouling, enhanced storage stability, and multimodality. Organically modified silica (ormosil) nanoparticles are a special type of hybrid nanoparticles known for encapsulating/conjugating active agents for applications such as in photodynamic therapy (PDT), gene therapy and diagnostic imaging. Herein, we report the use of ormosil nanoparticles as a sustained release drug delivery vehicle, using the well-known anticancer and fluorescent drug doxorubicin (Dox). These drug/dye loaded nanoparticles have been synthesized within an oil-in-water microemulsion medium, and characterized for their size, shape, porosity, and optical properties. Nanoencapsulation significantly enhanced the optical stability of a dye against chemical quenching. Particle-size variation could be achieved by changing the amount of co-surfactant. However, size variation did not affect their pore size. The release pattern of encapsulated drug was found to depend on the size of the nanoparticles, with optimal drug release observed for the 50 nm particles at about 70% in a sustained manner over two weeks. Confocal bioimaging was used to demonstrate the differential pattern of cellular uptake of the free and nanoencapsulated drugs, as the sub-cellular distribution of nanoencapsulated Dox is guided by the nanoparticles distributing throughout the cytosol. Cell viability (MTS) and soft-agar colony formation assays *in vitro* have confirmed the cytotoxic effects of the drug loaded nanoparticles, but not of the blank nanoparticles. The results indicate that ormosil nanoparticles can act as a sustained release vehicle of potent lipophilic anticancer drugs.

Keywords*: Oil-in-water microemulsion, ormosil nanoparticles, porosity, size-tunable drug release, cytotoxicity*

1. Introduction

Several drug delivery systems, which can render an aqueous dispersible formulation of poorly water soluble drugs, have emerged as potential clinical platforms over the past three decades.[1-4] They have numerous advantages over the conventional 'free' drug formulations, which include increased bioavailability and higher efficacy, target specificity, sustained drug release, minimal systemic or organ toxicity, etc. A gamut of drug categories, which include chemotherapeutics, immuno-suppressants, non-steroidal anti-inflammatory drugs (NSAIDs), antibiotics, anaesthetics, etc, can be re-formulated in combination with drug-delivery systems for clinically-relevant drug action.

Till now, majority of the sustained release drug delivery formulations have been based on liposomal and polymeric micro/nanoparticles.[5-7] Such macromolecular carriers either encapsulate (pre-load) the drugs during their synthetic stages, or adsorb (post-load) the drugs into their matrix after they are formed. The release mechanism of the drugs from the host matrix is via either surface erosion (in case of biodegradable carriers), or slow diffusion through the pores of the carrier.[8] Along with the capability of sustained drug release, such systems can also be engineered for preferential accumulation in target organs/tissues. As a result, several such formulations have been investigated in pre-clinical and clinical research, though in comparison very few of them are yet approved for routine clinical use.[9] A number of drawbacks have severely impeded the clinical translation of such 'soft' macromolecular drug carriers, which include large particle size (usually above 100 nm in diameter), structural and colloidal instability, poor shelf-life, vulnerability to biofouling, premature drug release, susceptibility to capture by the reticuloendothelial system (RES), potential immunogenicity, etc.[10]

An exciting alternative to 'soft' nanoparticles as drug carriers are porous inorganic nanomaterials, which have several advantages such as smaller particle size to enhance cellular uptake (diameter below 50 nm), higher shelf-life, resistance to biofouling, non-immunogenicity, etc. A popular example is the class of mesoporous silica nanoparticles (MSNs), with tunable diameter and pore-size (e.g. MCM-41, MCM-48, SBA-15, etc).[11-13] These nanoparticles can host a number of active agents within their large porous interior, which can later be released in a sustained and/or stimuli-sensitive manner.[14] In addition, the rich chemistry of silica makes possible the conjugation of a variety of stimuli-sensitive/diagnostic/biorecognition molecules on their surface, leading to the fabrication of multimodal nanoparticles with capability of site-specific delivery.[15-16] However, the large particle size (diameter above 100 nm), and colloidal instability of most MSNs are matters of concern for their biomedical

RSC Advances Accepted Manuscript

applications.[17-19]

Organically modified silica (ormosil) nanoparticles are an exciting class of hybrid materials with several promising applications.[20] Our research group has pioneered the biological applications of ormosil nanoparticles, encapsulated/conjugated with various active agents in a microemulsion medium.[16] By variation of microemulsion composition, their average diameter can be varied from as small as 15 nm to as big as 80 nm, with high degree of monodispersity in each case.[21] Their effectiveness has been demonstrated for a number of biomedical applications, such as in photodynamic therapy of cancer (using non drug-release formulations),[22-23] gene therapy (using surface complexation strategy)[24-25], targeted optical bioimaging (using encapsulated dyes)[26], *in vivo* bioimaging, clearance and non-toxicity (in mice)[27], as well as *in vivo* neuronal targeting (in Drosophila).[28] These studies have indicated that ormosil nanoparticles can serve as a versatile platform, which can be suitably modified to suit a variety of biomedical applications.

Herein, we have investigated the suitability of these nanoparticles as sustained release vehicles for lipophilic molecules, and examined if particle dimensions (size and pore volume) will have any effect on the pattern of drug release. We have studied the time dependent drug-release pattern from three different-sized ormosil nanoformulations (diameters 30, 50 and 80 nm) containing the fluorescent drug doxorubicin (Dox). Following physical and optical characterization of these doped nanoparticles, we have investigated their interaction with cultured cancer cells *in vitro*, beginning with visualizing their cellular uptake and intracellular localization, using fluorescence microscopy. Finally, using two independent cell viability (MTS and soft-agar colony formation) assays, we have probed both the absence of non-specific toxicity of blank nanopartices, and triggering of therapeutic toxicity by drug-doped nanoparticles in treated cells.

2. Materials and methods

2.1. Materials

The following chemicals were purchased from Sigma-Aldrich: surfactant aerosol OT (AOT), co-surfactant 1-butanol, ormosil precursor vinyltriethoxysilane (VTES), dyes ruthenium-tris (2,2′-bipyridyl) dichloride (RU), the drug doxorubicin hydrochloride (Dox), agarose and crystal violet. The pancreatic cancer cell line MiaPaCa-2 (ATCC No. CRL-1420) was obtained from ATCC, VA, and cultured according to instructions supplied by the vendor. The MTS reagent is a product of Promega. Unless otherwise mentioned, all other cell culture products, such as fetal bovine serum (FBS), phosphate buffer saline (PBS), dulbecco's modified eagle's medium (DMEM), penicillin, streptomycin and amphotericin-B, were obtained from Invitrogen.

2.2. Synthesis and purification of ormosil nanoparticles of different sizes, with and without encapsulated Dox or RU

The nanoparticles were synthesized in the non-aqueous core of an oil-in-water microemulsion system, by slight modification of our previously reported procedure.[21-22] Briefly, the microemulsion was prepared by dissolving 0.22 g of the surfactant AOT in 10 mL of water. This microemulsion is stabilized by the addition of the co-surfactant 1-butanol, whose amount dictated the final size of the nanoparticles (400µL, 600 µL and 800 µL of 1-butanol, for the small, medium and large size nanoparticles, respectively). Following this, 100 µL of aqueous ammonia solution and l00 µL either pure DMSO, or drug Dox dissolved in DMSO (34 mM), or dye RU dissolved in DMSO (5 mM), were sequentially dissolved in the microemulsion by vigorous magnetic stirring. The addition of aqueous ammonia was necessary to convert the water-soluble doxorubicin hydrochloride into its poorly water soluble doxorubicin form. To this system, 100 µL of neat VTES was added and the resulting solution was vigorously stirred for 1 hour. After this period, 10 µL of aqueous ammonia was added to the solution, and it was left stirring overnight for the formation of the nanoparticles. At the end of the synthesis process, the faint translucency developed in the solution indicated the formation of nanoparticles. Following the synthesis, the surfactant, co-surfactant, and other unreacted molecules were removed by dialysis against distilled water for about 48 hours, using a cellulose dialysis membrane with a cut off size of 12–14 kDa. At the end of dialysis, the nanoparticles were sterile filtered using 0.45 µm syringe filter and stored at 4°C for future use.

2.3. Characterization of nanoparticles, with and without encapsulated Dox/RU

Particle size was determined using transmission electron microscopy (TEM) and Dynamic light scattering (DLS). For TEM, the specimens were drop-coated and dried onto carbon coated 300 mesh copper grids, followed by imaging using a JEOL model JEM-100CX microscope with an acceleration voltage of 100 kV. DLS and surface charge measurements were carried out using a Brookhaven 90 Plus Zeta PALS Instrument. UV-vis absorption spectra and fluorescence emission spectra were recorded using a UV-Visible (Shimadzu UV-3600) spectrophotometer and a Fluorolog-3 (Jobin Yvon, Longjumeau, France) spectrofluorimeter, respectively.

The stability of the dye RU, both free and nanoencapsulated were studied using fluorescence quenching experiment. Here, fixed concentrations of free and nanoencapsulated dye in aqueous medium have been treated with various concentrations of the chemical quencher Cu^{2+} (copper sulfate). Fluorescence emission intensities in the absence (Io) and presence (I) of various quencher concentrations was then measured using the spectrofluorimeter. A plot was made with the ratio (I/Io) versus quencher concentration [Q]. The slope of the plot indicated the magnitude of chemical quenching of the dye.[29]

2.4. Nitrogen adsorption isotherm

Nitrogen adsorption isotherm studies were used to detect the surface area and porosity of the nanoparticles. Aqueous samples of nanoparticles were centrifuged at 20,000 rpm for one hour, and the precipitate collected and dried under a regular oven at 700^{0}C.

RSC Advances Accepted Manuscript

 This journal is © The Royal Society of Chemistry [year]

The dry powder was then degassed, and examined by N_2 adsorption isotherms at 77K and the related data calculated. Pore sizes were obtained from the isotherm by the Barret–Joyner–Halenda (BJH) method.[30] The BET analysis was performed in a Quanta chrome Nova Win Instrument (Quanta chrome Instruments), with data acquisition and reduction for NOVA instruments.

2.5. Drug-release studies

We have investigated the release behaviour of Dox from ormosil nanoparticles by dialyzing them in a solution containing Tween-80 micelles (1% in water) for two weeks. As owing to the low cut-off (12-14 kDa) pore size of the dialysis membrane only free Dox molecules can come out of the membrane, we have estimated the amount of released Dox by measuring the Dox concentration (via fluorescence spectrometry) in the bulk solution as a function of time of dialysis.

2.6. Cell Staining Studies

For *in vitro* imaging with free versus nanoencapsulated Dox, the human pancreatic cancer cell line MiaPaCa-2 was cultured in Dulbecco minimum essential media (DMEM) with 10% fetal bovine serum (FBS), 1% penicillin, and 1% amphotericin B. The day before nanoparticles treatment, cells were seeded in 35 mm culture dishes. On the treatment day, the cells, at a confluency of 70–80%, in serum-supplemented media were treated with free and nanoencapsulated Dox at a Dox concentration of 1 µM. After two hours, the cells were washed thrice with PBS and directly imaged using a Leica TCS SP2 AOBS spectral confocal microscope with laser excitation at 442 nm (Leica Microsystems Semiconductor GmbH, Wetzler, Germany). All images were taken under exact same conditions of laser power, aperture, gain, offset, scanning speed, and scanning area.

2.7. MTS Cell Viability Assay

The MiaPaCa-2 cells, cultured in Dulbecco minimum essential media (DMEM) with 10% fetal bovine serum (FBS), were dispensed into a 24-well cell culture plate (10,000 cells/well) and allowed to attach overnight. Next day, the cells were treated with the various samples (free Dox, placebo nanoparticles, and Dox-encapsulated nanoparticles) at final Dox concentrations of 1.2 and 2.4 µM, and placed back in the incubator for 2 days. Following the treatment period, the cells were washed, and cell viability was assessed by the Cell Titer-Glo luminescent cell viability assay (Promega Corporation, Madison, WI) following manufacturer's instructions. Luminescence was measured using a microplate luminometer (Bio-Tek Synergy HT microplate reader) and data were expressed as a percentage of the untreated control. Tests were performed in triplicate.

2.8. Soft-agar colony formation assay of MiaPaCa-2 cells

Briefly, 2 mL of mixture of serum supplemented medium and 0.5% agar treated with the various samples (free Dox, and Dox/ORM) with a final Dox conc. of 1.2 µM were added in a 35-mm culture dish and allowed to solidify (base agar). Next, on top of the base layer was added a mixture of serum supplemented medium and 0.35% agar (total of 2 mL) containing 5,000 cells, again treated with the various samples (free Dox, and Dox/ORM) with a final Dox conc. of 1.2 µM and allowed to solidify (top agar). Additional, non-Dox containing control sets consisted of either no treatment, or treatment with placebo ORM, under the same above conditions. Subsequently, 2 mL of media containing equivalent amount of the various samples and controls were added on top of their respective dishes, and the dishes were kept in tissue culture incubator maintained at 37°C and 5% CO_2 for 14 days to allow for colony growth. All assays were done in triplicate. The colony assay was terminated at day 14, when plates were stained with crystal violet, and photographed using a regular digital camera.

3. Results and Discussion

Our primary aim was to investigate if these nanoparticles can release the encapsulated doxorubicin in a sustained manner, and whether this release pattern will vary with the size of the nanoparticles. Therefore, we synthesized doxorubicin-encapsulated ORMOSIL nanoparticles of three different sizes, and analyzed their size using transmission electron microscopy (TEM). Fig. 1 (A-C) represents the TEM images of nanoparticles, with sizes of 30 nm (Fig. 1A), 50 nm (Fig. 1B) and 80 nm (Fig. 1C), for the small (ORM-S), medium (ORM-M) and larger (ORM-L) nanoparticles, respectively. All the nanoparticles within each batch are found to be spherical and highly monodispersed.

As these nanoparticles are intended for biological applications, we next investigated the effect of serum proteins on their hydrodynamic size, using dynamic light scattering (DLS). The samples were dispersed in both water and serum supplemented cell culture medium (DMEM with 10% FBS). As shown in Fig. 1D the hydrodynamic size of all the nanoparticles dispersed in water is somewhat bigger than that measured by TEM. This is because while TEM depicts the actual size of the nanoparticles, DLS shows their hydrodynamic size, with hydration layers surrounding the particle core, thus accounting for the increase in overall size. Furthermore, upon dispersing the nanoparticles in serum supplemented media, their hydrodynamic diameter further increased, which can be accounted for by the adsorption of serum proteins on the nanoparticle surface. Overall, this data confirms the small size, uniformity, and colloidal stability of the doped nanoparticles, even after adsorption of serum proteins in the biological milieu.

The surface charge of these nanoparticles, with and without Dox encapsulation, are provided in supplementary data (Supplementary 1). The nanoparticles have negative surface charge, which become less negative upon Dox encapsulation.

RSC Advances Accepted Manuscript

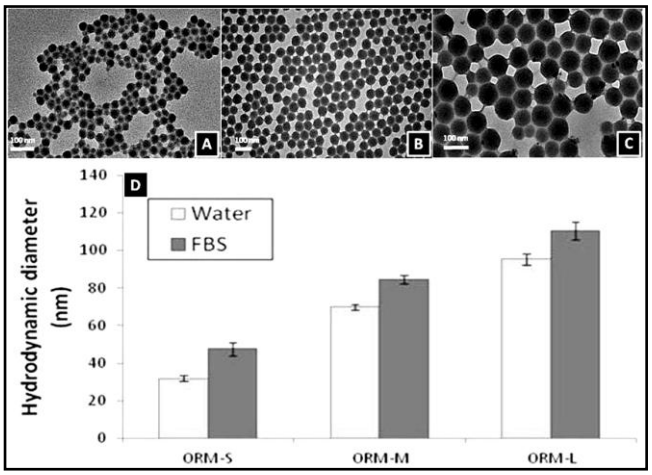

Figure 1: (A-C) TEM images of the (A) small, (B) medium, and (C) large Dox-loaded ORMOSIL nanoparticles, showing their uniformity of size. Scale bar = 200 nm and (D) Dynamic light scattering (DLS) data showing the hydrodynamic size of the ORMOSIL nanoparticles, dispersed in pure water as well as in serum-supplemented cell culture media.

Next, we studied the surface area and porosity of these nanoparticles using nitrogen adsorption isotherm. The BJH pore size distribution for the ORM-S, ORM-M and ORM-L nanoparticles are provided in Fig. 2. It is interesting to observe that both the surface area per unit mass (reported in m^2/g) and pore-diameter of the nanoparticles have no particular dependence on the variation of overall particle diameter. Previous reports about MSNs indicate that their surface area and pore size vary depending on the silica precursor and type of surfactant used (anionic/cationic/non-ionic).[11-14] In comparison, here only the amount of co-surfactant varies among the three batches. This variation, even though is causing noticeable changes in the overall diameter of the nanoparticles, do not seem to affect their surface area and pore diameter. Our results agree well with that reported by Lin et al., who observed that specific surface area per unit mass and pore diameter of mesoporous silica nanoparticles do not vary significantly upon changing their overall diameter.[31]

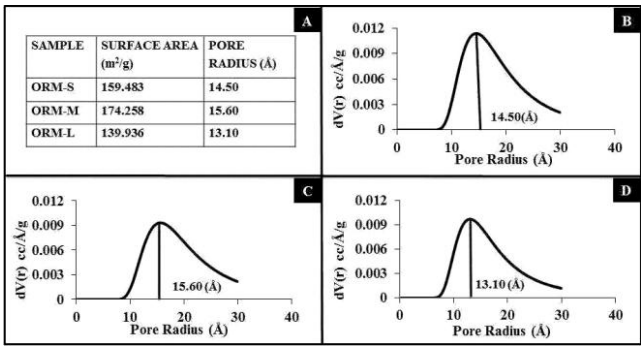

SAMPLE	SURFACE AREA (m^2/g)	PORE RADIUS (Å)
ORM-S	159.483	14.50
ORM-M	174.258	15.60
ORM-L	139.936	13.10

Figure 2: (A) Nitrogen adsorption isotherm results of ORM-S ,ORM-M and ORM-L nanoparticles, showing surface area and poreradius. (B, C, D) BJH pore size distribution curves for the ORM-S, ORM-M and ORM-L nanoparticles, respectively.

Next, we measured the fluorescence of aqueous dispersion of Dox-doped nanoparticles (Dox/ORM-S, Dox/ORM-M, and Dox/ORM-L) and compared them to that of free Dox dissolved in DMSO. All the four samples were excited with light of wavelength 470 nm (the absorption maxima for Dox), following normalization of their optical densities at this wavelength via UV-Visible spectrophotometry. Supplementary data (Supplementary 2) shows the fluorescence spectra of the samples, showing that the fluorescent properties of Dox are retained upon nanoencapsulation. Another optical characterization experiment carried out with the encapsulated dye RU yielded similar results (data not shown).

We then investigated whether nanoencapsulation enhances the stability of the dye RU against chemically-induced fluorescence quenching. From Fig. 3, it can be seen that the extent of fluorescence quenching of the free dye is more than that of the nanoencapsulated dyes, observed up to a quencher concentration as high as 15 mM. This indicates that the fluorescence of the free dye is more sensitive to chemical quenching than in their nanoencapsulated forms. In other words, nanoencapsulation enhances the optical stability of dye over that of the free one.

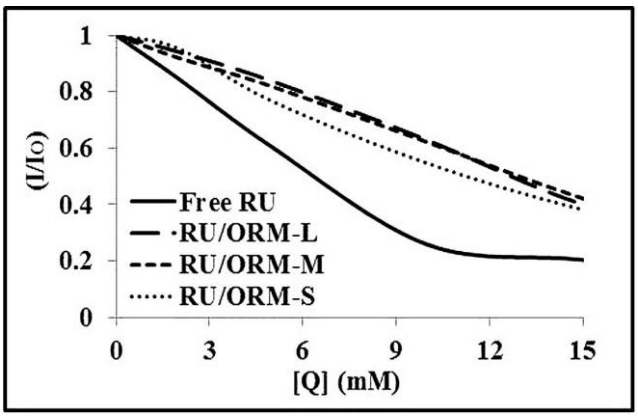

Figure 3: Chemically-induced fluorescence quenching data of dye RU, in free form (solid line) or encapsulated within ORM-S, ORM-M and ORM-L nanoparticles (dashed lines).

When Dox encapsulated nanoparticles are dispersed in completely aqueous environment, the poorly water soluble Dox molecules remain compacted within the inner core of the ormosil nanoparticles, where the organic groups provide them with local hydrophobic environment. However, when this external aqueous environment would also contain other hydrophobic hosts, such as micelles (*in situ*) or lipoproteins (*in vitro* and *in vivo*), it provides a driving force for the Dox molecules to be released from the nanoparticles, leading towards an equilibria where they are uniformly distributed within all the local hydrophobic microenvironments. We have investigated the time-dependent release behaviour of Dox from the nanoparticles by dialyzing them against Tween-80 micelles (1% in water). From Fig. 4, it can be seen that the drug is released from the nanoparticles in a sustained manner, with the release pattern being dependent on the

RSC Advances Accepted Manuscript

 This journal is © The Royal Society of Chemistry [year]

size of the nanoparticles. While the 30 nm particles poorly released the drug (about 40% release in two weeks), both the 50 nm and the 80 nm particles released about 70% of the total drug in the same time. However, the 50 nm particles released the drug in a more sustained manner, particularly at the initial period, while the 80 nm particles showed some burst-release behaviour. Thus, we concluded that the 50 nm particles showed the optimal drug-release pattern, and therefore used this formulation exclusively in the subsequent studies. This sustained release pattern is highly beneficial for controlled drug delivery applications.

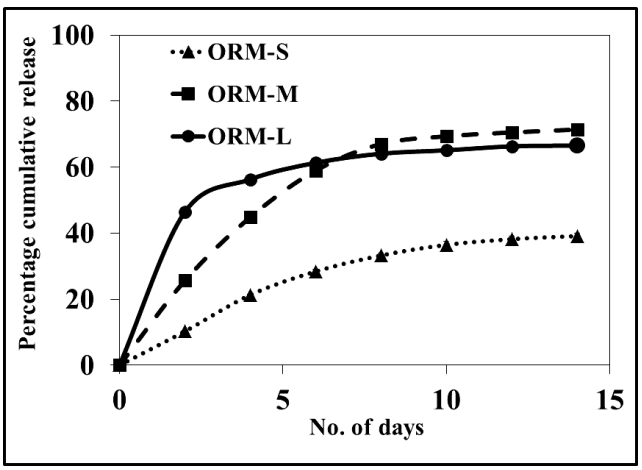

Figure 4: Release kinetics of Dox encapsulated modified silica nanoparticles, showing sustained release pattern, dependent on the overall size of the nanoparticles.

Next, using confocal bioimaging we investigated the uptake pattern of the Dox-encapsulated nanoparticles, as opposed to that of free Dox, in pancreatic cancer (MiaPaCa) cells treated for 2 hours. As shown in Fig. 5A, in cells treated with free Dox the drug is distributed in the cell membrane and the nucleus, with no appreciable drug content in the cytosol. This is because Dox, which is known for its high affinity for genetic materials owing to its cationic charge, freely diffuse into the cell nucleus and intercalate with the chromosomal DNA. In sharp contrast, the sub-cellular distribution of nanoencapsulated Dox is guided by the nanoparticles, which are shown distributed throughout the cytosol (Fig. 5B). No nuclear accumulation is observed in this case as these nanoparticles are not able to freely diffuse into the nucleus. The corresponding high resolution cellular images are also provided (Fig. 5C and 5D). Jain et al. have demonstrated similar confocal microscopic data of differential cellular distribution of free Dox versus Dox entrapped within the outer polymeric layer of iron-oxide nanoparticles.[32] This experiment serves as additional proof showing the difference between free and nanoencapsulated Dox. Scanning these treated cells under confocal microscopy was not possible for longer times post-treatment, owing to significant death of cells as a result of delivered Dox.

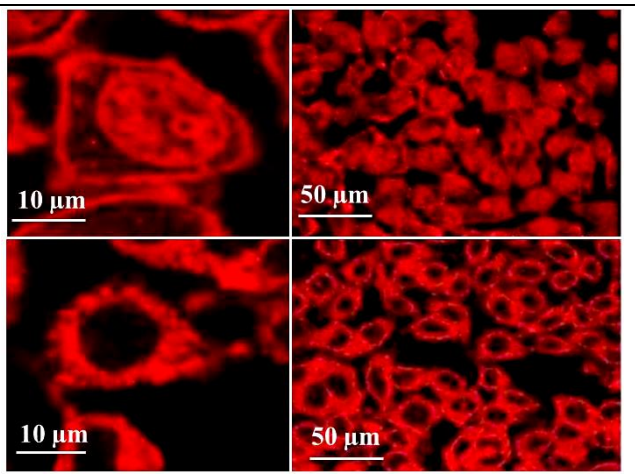

Figure 5: Confocal bioimaging of MiaPaCa cells treated with (A and B) free Dox and (C and D) nanoencapsulated Dox. Panels A and C: High resolution; and Panels B and D (low resolution) images.

After confirming the cellular uptake, we investigated the cytotoxic effect of free and nanoencapsulated Dox on MiaPaCa cells following 2 days of treatment. Fig. 6A represents the results of cell viability (MTS) assay of MiaPaCa cells following treatment with PBS, free Dox, Dox-encapsulated nanoparticles, and blank nanoparticles. The percentage viabilities of these treated cells are calculated relative to that of the cells undergoing treatment with PBS (assigned cell 100% viability). From this figure, it is evident that while placebo nanoparticles have no effect on the cell viability, the Dox-encapsulated nanoparticles caused about 90% cell death. This shows that while the nanoparticles themselves are non-toxic to the cells, the encapsulated drugs are released within the cells, which are responsible for the observed cytotoxicity. It may be noted that the cytotoxic efficacy of the Dox-encapsulated nanoparticles is slightly lower than that of free Dox, indicating that not all the Dox is released from the nanoparticles.

The cytotoxicity of the Dox-encapsulated nanoparticles was further confirmed using a soft-agar colony formation assay, which is a more stringent assay for cell viability. Here, the ability of MiaPaCa cells, either untreated, or treated with free Dox, placebo nanoparticles and Dox-encapsulated nanoparticles, to form colonies in soft-agar was examined for two weeks. As shown in the images of Fig. 6 (B-E), while untreated (Fig. 6B) and placebo (Fig. 6C) nanoparticle treated cells formed a number of colonies (dark spots in the plate), almost no colony was visible for cells treated with free Dox (Fig. 6D) and Dox-encapsulated nanoparticles (Fig. 6E). Owing to the lack of a colony-counting software, we are unable to provide a more quantitative estimate of the number of cell colonies in the plates. Nevertheless, this data serves as additional proof of loss of viability and normal functional ability of cancer cells upon treatment with Dox-encapsulated nanoparticles. These two cell viability experiments independently proved that for the same amount of the drug, the free and nanoencapsulated Dox have similar anticancer efficiency *in vitro*, as opposed to the placebo nanoparticles which show no evidence of cytotoxicity.

RSC Advances Accepted Manuscript

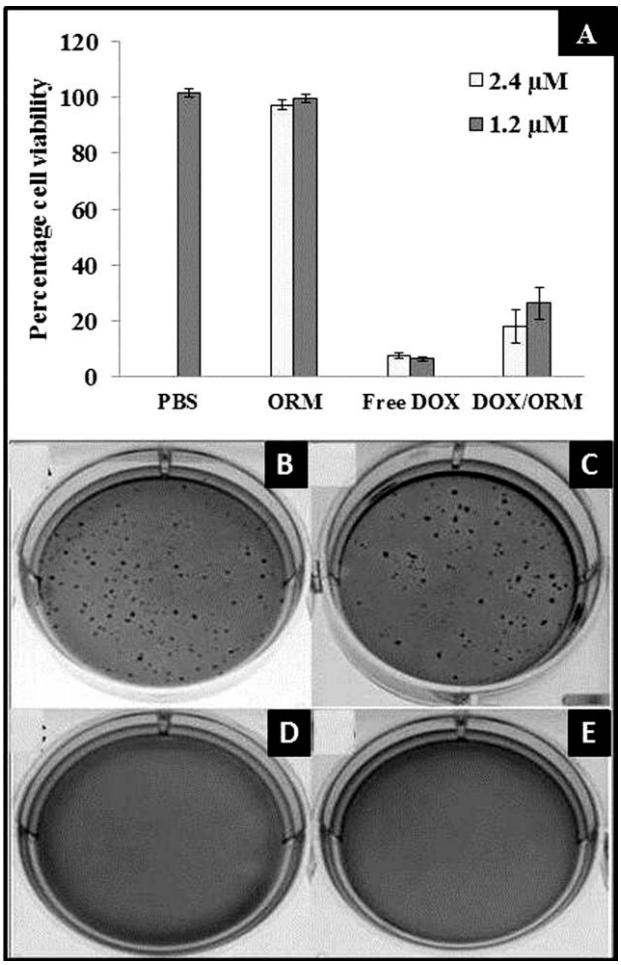

Figure 6: (A) Cell viability (MTS) assay showing while there is no cytotoxic effect of the non-drug loaded nanoparticles, potent cytotoxic effect has been observed with the drug-loaded nanoparticles in vitro, comparable to that of equivalent dosage of free Dox and (B-E) Photographic images of soft agar colony formation assay of MiaPaCa cells following their treatment with (B) PBS, (C) placebo nanoparticles, (D) free Dox and (E) Dox-loaded nanoparticles.

4. Conclusions

In conclusion, we have demonstrated the synthesis of highly monodispersed ormosil nanoparticles which encapsulate the lipophilic drug Dox, and release it in a sustained manner (~ 70% release in two weeks). These drug-encapsulated nanoparticles are robustly uptaken by cells in culture, and they subsequently exert potent therapeutic effect in the cells *in vitro*. From the point of view of cancer therapy, Dox-encapsulated ormosil nanoparticles are particularly attractive for additional therapeutics such as using co-encapsulated photosensitizers for photodynamic therapy (PDT) or attaching on their surface suicide genes for cancer gene therapy, which would allow multiple therapeutic regimens to act simultaneously and synergistically against cancer.

Acknowledgments

This study was mainly supported by a grant from the NCI/NIH (RO1 CA119397). The authors thank Dr. Tokeer Ahmad, Jamia Millia Islamia, Delhi, for his generous permission to allow us access to his BET experimental facility, and expert advice. IR is also thankful to Research and Development grant received from the University of Delhi, India.

Notes and references

[a] Department of Chemistry, University of Delhi, Delhi-110007, India. Email: indrajitroy11@gmail.com; Tel: +91-9560721851.
[b] Department of Chemistry and the Institute for Lasers, photonics and Biophotonics, State University of New York at Buffalo, Buffalo, NY-14226. Email: pnprasad@buffalo.edu; Tel: (716) 645-4147.
[c] School of Electrical and Electronic Engineering, Nanyang Technological University, 639798, Singapore.

† Electronic Supplementary Information (ESI) available: Zeta potential and Fluorescence spectra data. See DOI: 10.1039/b000000x/

[1]. S. S. Davis, *Trends in Biotechnology*, 1997, **15**, 217-224.
[2]. H. Devalapally, A. Chakilam and M. M. Amiji, *J. Pharm. Sci*., 2007, **96**, 2547-2565.
[3]. K. E. Uhrich, S. M. Cannizzaro, R. S. Langer and K. M. Shakesheff, *Chem .Rev*., 1999, **99**, 3181-3198.
[4]. E. R. Gillies and J. M. Frechet, *Drug .Discov today*, 2005, **10**, 35-43.
[5]. D. S. Kohane, J. Y. Tse, Y. Yeo, R. Padera, M. Shubina and R. Langer, J .Biomed. *Mater. Res. A*., 2006, **77**, 351-361.
[6]. A. N. Lukyanov and V. P. Torchilin, *Adv .Drug. Deliv. Rev*., 2004, **56**, 1273-1289.
[7]. L. E. V. Vlerken and M. M. Amiji, *Expert .Opin. Drug Deliv*., 2006, **3**, 205-216.
[8]. J. K. Vasir and V. Labhasetwar, *Adv .Drug. Deliv Rev*., 2007, **59**,718-728.
[9]. A. Z. Wang, R. Langer and O. C. Farokhzad, Annu. *Rev. Med*., 2012, **63**,185-198.
[10]. T. K. Jain, I. Roy, T. K. De and A. N. Maitra, *J. Am. Chem. Soc*., 1998, **120**,11092-11095.
[11]. F. Tang, L. Li and D. Chen, *Adv. Mater*., 2012, **24**, 1504–1534.
[12]. J. L. Vivero-Escoto, R. C. Huxford-Phillips and W. Lin, *Chem. Soc. Rev*., 2012, **41**, 2673–2685.
[13]. Y. Chen, H, Chen and J. Shi, *Adv. Mater*., 2013, **25**, 3144-3176.
[14]. Z. Li, J. C. Barnes, A. Bosoy, J. F. Stoddart and J. I. Zink, *Chem. Soc. Rev*., 2012, **41**, 2590–2605.
[15]. R. K. Sharma, S. Das and A. N. Maitra, *J. Colloid. Interface. Sci*., 2004, **277**, 342-346.
[16]. P. N. Prasad, *Introduction to Biophotonics*. Wiley: New York .2004.

RSC Advances Accepted Manuscript

 This journal is © The Royal Society of Chemistry [year]

[17]. M. Vallet-Regí, F. Balas and D. Arcos, *Angew. Chem. Int. Ed Engl*., 2007, **46**, 7548–7558.
[18]. M. W. Ambrogio, C. R. Thomas, Y. L. Zhao, J. I. Zink and J. F. Stoddart, *Acc. Chem. Res*., 2011, **44**, 903–913.
[19]. D. Douroumis, I. Onyesom, M. Maniruzzaman and J. Mitchell, *Crit. Rev. Biotechnol*., 2013, **33**, 229-245.
[20]. S. J. Das, T. K. Jain and A. N. Maitra, *J. Colloid Interface Sci*., 2002, **252**, 82-88.
[21]. I. Roy, T. Y. Ohulchanskyy, D. J. Bharali, H. E. Pudavar, R. A. Mistretta, N. Kaur and Paras. N. Prasad. *Proc. Natl. Acad. Sci. USA*., 2005, **102**, 279-284.
[22]. I. Roy, T. Y. Ohulchanskyy, H. E. Pudavar, E. J. Bergey, A. R. Oseroff, J. Morgan, T. J. Dougherty and P. N. Prasad, *J. Am. Chem .Soc*., 2003, **125**, 7860-7865.
[23]. T. Y. Ohulchanskyy, I. Roy, L. N. Goswami, Y. Chen, E. J. Bergey, R. K. Pandey, A. R. Oseroff and P. N. Prasad, *Nano Lett*., 2007, **7**, 2835-2842.
[24]. D. J. Bharali, I. Klejbor, E. K. Stacowiak, P. Dutta, I. Roy, N. Kure , E. J. Bergey, P. N. Prasad and M. K. Stachowiak, *Proc. Natl. Acad. Sci. USA*., 2005, **102**, 11539-11544.
[25]. I. Roy, M. K. Stachowiak and E. J. Bergey, *Nanomedicine*., 2008, **4**, 89-97.
[26]. R. Kumar, I. Roy, T. Y. Ohulchanskyy, L. N. Goswami. A. C. Bonoiu, E. J. Bergey, K. M. Tramposch, A. Maitra and P. N. Prasad, *ACS Nano*., 2008, **2**, 449-456.
[27]. R. Kumar, I. Roy, T. Y. Ohulchanskky, L. A. Vathy, E. J. Bergey, M. Sajjad and P. N. Prasad, *ACS Nano*., 2010, **23**, 699-708.
[28]. F. Barandeh, P. L. Nguyen, R. Kumar, G. J. Iacobucci, M. L. Kuznicki, A. Kosterman, E. J. Bergey, P. N. Prasad and S. Gunawardena, *PLOS One*., 2012, **7**, e29424.
[29]. P. Kumar, Anuradha and I. Roy, *RSC Adv.*, 2014, **4**, 16181-16187.
[30]. J. F. Chen, H. M. Ding, J. X. Wang and L. Shao, *Biomaterials*., 2004, **25**, 723-727.
[31]. Y. S. Lin and C.L. Haynes, *J. Am. Chem. Soc*., 2010, **132**, 4834–4842.
[32]. T. K. Jain, M. K. Reddy, M. A. Morales, S. K. Sahoo, D. L. Leslie-Pelecky and V. Labhasetwar, *Molecular Pharmaceutics*., 2008, **2**, 194-205.

RSC Advances Accepted Manuscript